Relativistic coupled-cluster calculations of the polarizabilities of atomic thallium

Yong-Bo Tang,[1,2] Ning-Ning Gao,[1] Bing-Qiong Lou,[1] and Ting-Yun Shi[2]

[1]*College of Physics and Electronic Engineering, Henan Normal University, Xinxiang 453007, People's Republic of China*

[2]*State Key Laboratory of Magnetic Resonance and Atomic and Molecular Physics, Wuhan Institute of Physics and Mathematics, Chinese Academy of Sciences, Wuhan 430071, People's Republic of China*

(Received 21 August 2018; published 14 December 2018)

Using the relativistic coupled-cluster method, we calculate the static dipole polarizabilities of the $6p$, $7s$, $7p$, $8s$, $8p$, and $6d$ states and the dynamic dipole polarizabilities of the $6p$ and $7s$ states of the thallium atom. The trivalent thallium atom is computationally treated as a monovalent system, together with all linear and nonlinear terms of single- and double-cluster operators included in the correlation calculations. We observe that the dominating contributions to the static scalar polarizabilities of the $7s_{1/2}$, $7p_{1/2}$, $8p_{1/2}$, and $8p_{3/2}$ states are from one or two specific transitions. The matrix elements of these specific transitions can be determined by combining the experimental values of relevant static scalar polarizabilities. A number of magic wavelengths for the $6p_{1/2}$–$7s$ and $6p_{3/2}$–$7s$ transitions in the range of 488–1300 nm and the longest tune-out wavelength of the ground state are determined. These magic wavelengths and tune-out wavelength may be useful for further thallium experiments. Experimental measurements of the magic wavelengths near 1245 nm would give estimates of the $7s_{1/2}$–$7p_{1/2}$ and $7s_{1/2}$–$7p_{3/2}$ transition matrix elements and their ratio. Furthermore, lifetimes of many excited states, as well as the Stark-induced scalar and vector dipole polarizabilities for the $6p_{1/2}$–$7p_{1/2}$ transition, are also evaluated and compared with available theoretical and experimental values.

DOI: 10.1103/PhysRevA.98.062511

I. INTRODUCTION

The polarizability of an atom or ion can be considered as a measure of response of the atomic charge cloud to an external electric field [1]. Studies of polarizabilities for atoms and ions are very important in many areas of physics. For example, static polarizabilities are required for evaluating the blackbody radiation (BBR) shift of a clock state, which could be significant for the uncertainty budget of an atomic clock [2,3]. Dynamic polarizabilities can be used to identify magic wavelengths of an atomic transition and tune-out wavelengths of an atomic state. The identification of magic wavelengths and their use in making optical lattices have resulted in the development of optical lattice clocks [4,5]. Knowledge of magic wavelengths are also very useful for laser cooling and trapping of atoms and for high-precision measurements [6–9]. The concept of tune-out wavelength has been applied to multispecies atomic trapping [10,11]. Because the polarizability-related shifts are equal to zero at the magic and tune-out wavelengths, it should be possible to measure these wavelengths to high precision. Measurements of these wavelengths open a route to determine electron dipole transition matrix elements (E1) of some specific transitions or the ratios between these matrix elements [12–15]. At the same time, it also provides an opportunity for testing atomic structure theories [16–18].

The atomic thallium, the heaviest element of the IIIA group of the periodic table, has played an important role in studying atomic parity nonconservation (PNC) [19–21] and the electron's electric dipole moment (e-EDM) [22,23]. Knowledge of polarizabilities, magic wavelengths, and tune-out wavelengths of Tl may be useful for further PNC, e-EDM and related high-precision measurements based on Tl atom. The present work reports calculations of the static dipole polarizabilities of the $6p$, $7s$, $7p$, $8s$, $8p$, and $6d$ states and the dynamic dipole polarizabilities of the $6p$ and $7s$ states of Tl. A number of magic wavelengths for the $6p_{1/2}$–$7s$ and $6p_{3/2}$–$7s$ transitions and the longest tune-out wavelength of the ground state are given.

There have been several reported works for the polarizabilities of Tl [21,22,24–29]. The Stark-induced amplitudes of the $6p_{1/2}$–$7p_{1/2}$ transition have been measured by Tanner and Commins [24], and by Demille *et al.* [25]. Doret *et al.* measured the scalar Stark shift in the $6p_{1/2}$–$7s_{1/2}$ transition using a Tl atomic beam apparatus and a stabilized frequency-doubled diode laser system [26]. On the theoretical side, Kozlov *et al.* used the relativistic configuration interaction plus many-body perturbation theory (RCI+MBPT) to evaluate the scalar and tensor dipole polarizabilities of the $6p_{1/2}$ and $6p_{3/2}$ states of Tl [21]. Safronova *et al.* calculated the Stark-induced dipole scalar and vector polarizabilities for $6p_{1/2}$–$7p_{1/2}$ using a relativistic all-order method [27], which is equivalent to the linear version of the coupled-cluster method (LCCSD). Dzuba and Flambaum reported the scalar dipole polarizabilities of the ground state of Tl using the RCI+MBPT method [22]. Borschevsky *et al.* employed a finite field coupled-cluster method to calculate the static dipole polarizabilities of the $6p_{1/2}$ and $6p_{3/2}$ states of Tl [28]. Recently the all-order method and a hybrid method combing configuration interaction and the all-order method were used to calculate the static scalar polarizabilities of the $6p_{1/2}$, $7s_{1/2}$, and $7p_{1/2}$ states of Tl [29], and the $7p$ state lifetimes were extracted by comparing an existing Tl Stark shift measurement [26]. These works have mainly focused on the static polarizabilities of the first few low-lying states. Recently,

the polarizabilities of the $6p$ and $7p$ states of the atomic indium have been measured accurately by using the two-step diode laser spectroscopy, which can be extended to Tl [30,31]. Therefore, theoretical investigation of $7p$ and $8p$ states' static polarizabilities of Tl are interesting. To our knowledge, no theoretical calculations of the dynamic polarizabilities of Tl are available in the literature.

Accurate theoretical predictions for atomic properties of Tl require a powerful relativistic many-body method, which should treat relativistic and electron-electron correlation effects on the same footing. Tl is nominally a trivalent atomic system with the ground-state configuration being $6s^2_{1/2}6p_{1/2}$. An exact calculation of this trivalent system needs to include the core-core, core-valence, and valence-valence correlations, which demands huge computation sources. We thus approximate Tl as a monovalent atomic system with the close-shell core being Xe ($6s^2$), as in Refs. [27,32]. Comparing to the all-order method used in Refs. [27,32], here we use a relativistic coupled-cluster method at single and double approximation (RCCSD) that includes all linear and nonlinear terms. The nonlinear terms account for the contributions from many of the triple and quadruple determinantal states, which is necessary for achieving high accurate results. Gharibnejad and Derevianko have calculated atomic properties of some low-lying states of boron, the lightest member of the IIIA group elements, using the RCC method at various approximations [33]. Their results have demonstrated that the higher order correlation beyond LCCSD, in particular the correlations from the nonlinear terms, are essential for obtaining high accurate results.

This paper is organized as follows. The theoretical formulation of the coupled-cluster method is given in Sec. II. Numerical results are presented in Sec. IV, together with comparisons with available experimental and theoretical data. Finally, a summary is given in Sec. V. Atomic units are used throughout unless otherwise stated.

II. THEORETICAL FORMULATION

A. Polarizabilities

The dynamic dipole polarizability of a state $|\Psi_v\rangle$ at photon energy ω is defined by

$$\alpha_0^{(1)}(\omega) = \frac{2}{3(2J_v+1)} \sum_i \frac{|\langle \Psi_i \| D \| \Psi_v \rangle|^2 \varepsilon_{iv}}{\varepsilon_{iv}^2 - \omega^2}, \tag{1}$$

where ε_{iv} represents the transition energy between states i and v and the summation runs over all intermediate states with allowed $\langle \Psi_i \| D \| \Psi_v \rangle$ electric dipole transitions. The dipole polarizability has a tensor component if $J_v > 1/2$, which can be written as

$$\alpha_{\rm t}^{(1)}(\omega) = 4\left[\frac{5J_v(2J_v-1)}{6(J_v+1)(2J_v+1)(2J_v+3)}\right]^{1/2} \times \sum_{J_i} (-1)^{J_v+J_i} \begin{Bmatrix} J_v & 1 & J_i \\ 1 & J_v & 2 \end{Bmatrix} \frac{|\langle \Psi_i \| D \| \Psi_v \rangle|^2 \varepsilon_{iv}}{\varepsilon_{iv}^2 - \omega^2}. \tag{2}$$

The polarizability for a state with nonzero angular momentum J_v depends on the magnetic projection M_v,

$$\alpha_{M_v}^{(1)}(\omega) = \alpha_0^{(1)}(\omega) + \alpha_{\rm t}^{(1)}(\omega) \frac{3M_v^2 - J_v(J_v+1)}{J_v(2J_v-1)}. \tag{3}$$

The dynamic polarizability is reduced to the static one if $\omega = 0$. The polarizability includes the contributions from the core, core-valence, and valence correlations, i.e., $\alpha^{(1)} = \alpha_c^{(1)} + \alpha_{cv}^{(1)} + \alpha_v^{(1)}$. In this work, $\alpha_c^{(1)} = 19.6$ was used, which was taken from the CI + all-order calculation by Zuhrianda *et al.* [34]. The main contributions are from the low-lying intermediate states, which were calculated using the RCCSD method. For the contributions from the core-valence correlation, higher-lying states, and the continuum, we evaluate them by employing the Dirac-Fock plus core potential (DFCP) method [14,35].

B. The coupled-cluster theory

In the coupled-cluster framework, the exact wave function for an atomic system with a valence orbital v can be expressed as

$$|\Psi_v\rangle = e^S |\Phi_v\rangle, \tag{4}$$

where $|\Phi_v\rangle$ is the reference state that can be taken as the lowest-order Dirac-Hartree-Fock wave function, and S is the cluster operator that can be expressed as a sum of n-particle excitation S_n of the lowest-order wave function,

$$S = \sum_{n=1}^{N} S_n, \tag{5}$$

with N the number of electrons in the system. In the coupled-cluster method at single and double approximation (CCSD) used here, the wave function of the system is simplified to the form,

$$|\Psi_v\rangle = \left[1 + S_1 + S_2 + \frac{1}{2}\left(S_1^2 + S_2^2 + 2S_1S_2\right) + \frac{1}{3!}\left(S_1^3 + 3S_1^2S_2\right) + \frac{1}{4!}S_1^4\right]|\Phi_v\rangle. \tag{6}$$

According to the number of valence holes and the number of valence particles to be excited with respect to the reference determinant, the cluster operator S can be partitioned into

$$S = S^{(0,0)} + S^{(0,1)} = S_1^{(0,0)} + S_2^{(0,0)} + S_1^{(0,1)} + S_2^{(0,1)}. \tag{7}$$

$S^{(0,0)}$ and $S^{(0,1)}$ correspond to the excitation from the core and from the valence electrons, respectively. In the language of second quantization, the cluster operator for the core excitation is

$$S^{(0,0)} = S_1^{(0,0)} + S_2^{(0,0)} = \sum_{ra} \{a_r^\dagger a_a\} s_a^r + \frac{1}{2}\sum_{rsab} \{a_r^\dagger a_s^\dagger a_a a_b\} s_{ab}^{rs}, \tag{8}$$

and the cluster operator for the valence excitation is

$$S^{(0,1)} = S_1^{(0,1)} + S_2^{(0,1)} = \sum_{r\neq v} \{a_r^\dagger a_v\} s_v^r + \sum_{rsa} \{a_r^\dagger a_s^\dagger a_v a_a\} s_{va}^{rs}. \tag{9}$$

In the above, the subscripts a and b denote the core orbitals, r and s the virtual orbitals, and v the valence state. Also in the above, $a^\dagger$ and a are, respectively, the single-particle creation and annihilation operators, and $s^{\cdots}_{\cdots}$ are the cluster amplitudes. These cluster amplitudes are obtained by iterating the coupled equations for the cluster operators. In practice, the equation for the $S^{(0,0)}$ is first solved iteratively until a convergence is reached. The sector $S^{(0,1)}$ is then solved using the known $S^{(0,0)}$. In this work, we use the direct inversion of iterative space (DIIS) [36,37] to accelerate the convergence.

After obtaining the cluster amplitudes, the transition matrix element of a one-particle operator Z between Ψ_w and Ψ_v can be evaluated according to

$$Z_{wv} = \frac{\langle\Psi_w|Z|\Psi_v\rangle}{\sqrt{\langle\Psi_w|\Psi_w\rangle\langle\Psi_v|\Psi_v\rangle}} = \frac{\langle\Phi_w|e^{S^\dagger}Ze^S|\Phi_v\rangle}{\sqrt{\langle\Phi_w|e^{S^\dagger}e^S|\Phi_w\rangle\langle\Phi_v|e^{S^\dagger}e^S|\Phi_v\rangle}}. \quad (10)$$

One may note that this expansion gives rise to an infinite number of terms. Thus, in practice, we just take account of the linearized expansion of the coupled-cluster wave functions with single and double excitations, which produces a finite number of terms:

$$\begin{aligned} e^{S^\dagger}Ze^S \approx{}& Z + \{S_1^{(0,0)\dagger}Z + \text{h.c.}\} + \{S_1^{(0,1)\dagger}Z + \text{H.c.}\} \\ &+ \{S_2^{(0,1)\dagger}Z + \text{h.c.}\} + \{S_1^{(0,0)\dagger}ZS_1^{(0,1)} + \text{H.c.}\} \\ &+ S_1^{(0,0)\dagger}ZS_1^{(0,0)} + \{S_1^{(0,0)\dagger}ZS_2^{(0,0)} + \text{H.c.}\} \\ &+ \{S_1^{(0,0)\dagger}ZS_2^{(0,1)} + \text{h.c.}\} + S_2^{(0,0)\dagger}ZS_2^{(0,0)} \\ &+ \{S_2^{(0,0)\dagger}ZS_2^{(0,1)} + \text{h.c.}\} + S_1^{(0,1)\dagger}ZS_1^{(0,1)} \\ &+ \{S_1^{(0,1)\dagger}ZS_2^{(0,1)} + \text{h.c.}\} + S_2^{(0,1)\dagger}ZS_2^{(0,1)}, \end{aligned} \quad (11)$$

and

$$\begin{aligned} e^{S^\dagger}e^S \approx{}& 1 + S_1^{(0,0)\dagger}S_1^{(0,0)} + S_1^{(0,1)\dagger}S_1^{(0,1)} \\ &+ S_2^{(0,0)\dagger}S_2^{(0,0)} + S_2^{(0,1)\dagger}S_2^{(0,1)}, \end{aligned} \quad (12)$$

where H.c. stands for the Hermitian conjugated part. In our previous work [38], we used this approximation to evaluate transition properties of atomic francium, where a comparison with available experimental data showed that this approximation can offer precise results.

III. COMPUTATIONAL DETAILS

In the Dirac-Hartree-Fock formalism, the large and small components of the radial wave functions are expanded using 50 B splines of order $k = 15$ defined on the finite domain [0,200]. The knot sequence of B splines satisfies an exponential distribution [39]. The Fermi nuclear distribution is used to describe the Coulomb potential between electrons and the nucleus. The Breit interaction is considered on the same footing as the electron-electron Coulomb interaction. The details of the Dirac-Fock calculation based on the B-spline basis are given in Refs. [35,38]. For the electron correlations, virtual orbitals with the energy smaller than 1500 and the partial wave $\ell_{\max} \leqslant 6$ are included in the calculation. In DFCP calculation, 70 B splines of order 15 were used, and the size of the B-spline domain was set to be 300.

TABLE I. Theoretical and experimental energy levels of Tl in cm^{-1}. E_{DF} and E_{CCSD} are the energies obtained using the DF and CCSD approximations, respectively. $\delta = |E_{\text{Expt}} - E_{\text{CCSD}}|/E_{\text{Expt}}$.

Level	E_{DF}	E_{CCSD}	E_{Expt} [40]	$\delta(\%)$
$6p_{1/2}$	−43710.38	−49179.94	−49266.66	0.18
$6p_{3/2}$	7107.93	7647.22	7792.70	1.87
$7s_{1/2}$	22611.31	26359.84	26477.50	0.44
$7p_{1/2}$	29448.59	34091.51	34159.90	0.20
$7p_{3/2}$	30359.77	35081.01	35161.10	0.23
$6d_{3/2}$	31492.26	36029.17	36117.90	0.25
$6d_{5/2}$	31542.29	36116.02	36199.93	0.23
$8s_{1/2}$	33673.90	38652.33	38745.90	0.24
$8p_{1/2}$	36117.29	41289.88	41368.10	0.19
$8p_{3/2}$	36464.19	41658.67	41740.80	0.20
$7d_{3/2}$	36845.85	41938.70	42011.40	0.17
$7d_{5/2}$	36872.59	41980.24	42049.00	0.16
$5f_{7/2}$	36847.29	42229.39	42318.44	0.21
$5f_{5/2}$	36847.43	42229.56	42318.44	0.21
$9s_{1/2}$	37818.86	43077.27	43166.20	0.21
$9p_{1/2}$	38972.05	44298.98	44380.90	0.18
$9p_{3/2}$	39142.57	44478.47	44562.50	0.19
$8d_{3/2}$	39319.46	44599.11	44672.60	0.16
$8d_{5/2}$	39334.36	44621.16	44692.70	0.16
$6f_{7/2}$	39317.17	44736.78	44823.52	0.19
$6f_{5/2}$	39317.28	44736.93	44823.52	0.19
$10s_{1/2}$	39833.33	45192.35	45296.80	0.23
$10p_{1/2}$	40468.30	45858.09	45939.30	0.18
$10p_{3/2}$	40564.85	45959.08	46043.60	0.18
$9d_{3/2}$	40661.87	46022.38	46098.50	0.17
$9d_{5/2}$	40670.86	46035.32	46110.30	0.16
$7f_{7/2}$	40659.48	46098.55	46185.25	0.19
$7f_{5/2}$	40659.56	46098.65	46185.25	0.19
$11s_{1/2}$	40965.25	46369.63	46456.90	0.19
$11p_{1/2}$	41351.79	46772.17	46853.80	0.17
$11p_{3/2}$	41411.76	46834.63	46917.10	0.18
$10d_{3/2}$	41470.92	46872.11	46949.90	0.17
$10d_{5/2}$	41476.71	46880.33	46958.00	0.17
$8f_{7/2}$	41468.98	46918.75	47004.55	0.18
$8f_{5/2}$	41469.04	46918.82	47004.55	0.18

IV. RESULTS AND DISCUSSIONS

A. Energies

The energy levels for the ns ($n = 7$–11), np ($n = 6$–11), nd ($n = 6$–10), and nf ($n = 5$–8) states of Tl are calculated using the relativistic coupled-cluster method in single and double approximation. In Table I, we present the DF energies (denoted by E_{DF}) and CCSD energies (denoted by E_{CCSD}), and compare with available experimental values from NIST [40]. The energies of excited states are present as the differences between the excited and ground states. δ is the relative difference between theoretical and experimental values $\delta = |E_{\text{Expt}} - E_{\text{CCSD}}|/E_{\text{Expt}}$. From Table I, one can find that our CCSD method gives fairly accurate results. The fine

TABLE II. Reduced electric-dipole matrix elements of Tl. Z_{DF}, and Z_{CCSD} are the results obtained using the DF and CCSD approximations, respectively. Z_{LCCSD} results are from all-order calculations by Safronova *et al.* [32].

Transitions	Z_{DF}	Z_{CCSD}	Z_{LCCSD} [32]	Transitions	Z_{DF}	Z_{CCSD}	Z_{LCCSD} [32]	Transitions	Z_{DF}	Z_{CCSD}
$6p_{1/2}$–$7s_{1/2}$	2.057	1.811	1.820	$7p_{1/2}$–$8s_{1/2}$	6.503	6.213	6.251	$8s_{1/2}$–$9p_{3/2}$	3.067	2.959
$6p_{3/2}$–$7s_{1/2}$	3.970	3.399	3.395	$7p_{3/2}$–$8s_{1/2}$	11.06	10.53	10.62	$8s_{1/2}$–$10p_{1/2}$	0.685	0.656
$6p_{1/2}$–$8s_{1/2}$	0.645	0.540	0.531	$7p_{1/2}$–$9s_{1/2}$	1.339	1.285	1.272	$8s_{1/2}$–$10p_{3/2}$	1.470	1.420
$6p_{3/2}$–$8s_{1/2}$	0.978	0.803	0.774	$7p_{3/2}$–$9s_{1/2}$	1.719	1.630	1.585	$8s_{1/2}$–$11p_{1/2}$	0.409	0.389
$6p_{1/2}$–$9s_{1/2}$	0.366	0.302	0.299	$7p_{1/2}$–$6d_{3/2}$	11.99	10.77	10.58	$8s_{1/2}$–$11p_{3/2}$	0.925	0.893
$6p_{3/2}$–$9s_{1/2}$	0.533	0.428	0.414	$7p_{3/2}$–$6d_{3/2}$	5.395	4.843	4.747	$8p_{1/2}$–$10s_{1/2}$	2.314	2.235
$6p_{1/2}$–$6d_{3/2}$	2.734	2.423	2.374	$7p_{3/2}$–$6d_{5/2}$	16.29	14.68	14.40	$8p_{1/2}$–$11s_{1/2}$	1.141	1.104
$6p_{3/2}$–$6d_{3/2}$	1.636	1.432	1.419	$7p_{1/2}$–$7d_{3/2}$	4.181	4.691	4.761	$8p_{1/2}$–$9d_{3/2}$	3.093	3.401
$6p_{3/2}$–$6d_{5/2}$	4.850	4.222	4.169	$7p_{3/2}$–$7d_{3/2}$	2.683	2.869	2.926	$8p_{1/2}$–$10d_{3/2}$	2.020	2.178
$6p_{1/2}$–$7d_{3/2}$	1.451	1.165	1.130	$7p_{3/2}$–$7d_{5/2}$	7.857	8.356	8.520	$8p_{3/2}$–$9d_{3/2}$	1.825	1.920
$6p_{3/2}$–$7d_{3/2}$	0.781	0.626	0.611	$7p_{1/2}$–$8d_{3/2}$	2.198	2.344	2.360	$8p_{3/2}$–$9d_{5/2}$	5.366	5.635
$6p_{3/2}$–$7d_{5/2}$	2.326	1.859	1.810	$7p_{3/2}$–$8d_{3/2}$	1.251	1.272	1.282	$8p_{3/2}$–$10d_{3/2}$	1.136	1.173
$6p_{1/2}$–$8d_{3/2}$	0.949	0.728	0.700	$7p_{3/2}$–$8d_{5/2}$	3.695	3.757	3.788	$8p_{3/2}$–$10d_{5/2}$	3.353	3.462
$6p_{3/2}$–$8d_{3/2}$	0.491	0.378	0.366	$6d_{3/2}$–$5f_{5/2}$	15.81	13.64	13.30	$6d_{3/2}$–$7f_{5/2}$	2.788	2.826
$6p_{3/2}$–$8d_{5/2}$	1.466	1.125	1.087	$6d_{5/2}$–$5f_{5/2}$	4.266	3.705	3.615	$6d_{3/2}$–$8f_{5/2}$	1.841	1.903
$7s_{1/2}$–$7p_{1/2}$	6.618	6.019	5.904	$6d_{3/2}$–$6f_{5/2}$	5.144	5.007	4.973	$6d_{3/2}$–$9f_{5/2}$	1.347	1.407
$7s_{1/2}$–$7p_{3/2}$	8.797	8.062	7.871	$6d_{5/2}$–$6f_{5/2}$	1.372	1.340	1.331	$6d_{5/2}$–$5f_{7/2}$	19.08	16.57
$7s_{1/2}$–$8p_{1/2}$	0.801	0.695	0.722	$6p_{1/2}$–$10s_{1/2}$	0.248	0.203		$6d_{5/2}$–$6f_{7/2}$	6.135	5.990
$7s_{1/2}$–$8p_{3/2}$	1.627	1.471	1.502	$6p_{1/2}$–$11s_{1/2}$	0.184	0.150		$6d_{5/2}$–$7f_{5/2}$	0.740	0.752
$7s_{1/2}$–$9p_{1/2}$	0.350	0.289	0.306	$6p_{1/2}$–$9d_{3/2}$	0.688	0.515		$6d_{5/2}$–$7f_{7/2}$	3.309	3.361
$8p_{1/2}$–$9s_{1/2}$	12.64	12.24	12.33	$6p_{1/2}$–$10d_{3/2}$	0.531	0.390		$6d_{5/2}$–$8f_{5/2}$	0.487	0.504
$8p_{3/2}$–$9s_{1/2}$	20.88	20.23	20.42	$6p_{3/2}$–$10s_{1/2}$	0.356	0.283		$6d_{5/2}$–$8f_{7/2}$	2.179	2.255
$8p_{1/2}$–$6d_{3/2}$	3.706	3.002	2.812	$6p_{3/2}$–$11s_{1/2}$	0.262	0.207		$6d_{5/2}$–$9f_{5/2}$	0.356	0.372
$8p_{3/2}$–$6d_{3/2}$	1.177	0.908	0.821	$7s_{1/2}$–$9p_{3/2}$	0.796	0.708		$6d_{5/2}$–$9f_{7/2}$	1.591	1.664
$8p_{3/2}$–$6d_{5/2}$	3.657	2.891	2.631	$7s_{1/2}$–$10p_{1/2}$	0.212	0.169		$5f_{5/2}$–$7d_{3/2}$	24.57	24.85
$8p_{1/2}$–$7d_{3/2}$	24.04	22.71	22.59	$7s_{1/2}$–$10p_{3/2}$	0.507	0.446		$5f_{7/2}$–$7d_{5/2}$	29.27	29.60
$8p_{3/2}$–$7d_{3/2}$	10.89	10.22	10.16	$7s_{1/2}$–$11p_{1/2}$	0.148	0.115		$5f_{5/2}$–$7d_{5/2}$	6.545	6.620
$8p_{3/2}$–$7d_{5/2}$	32.81	30.88	30.70	$7s_{1/2}$–$11p_{3/2}$	0.364	0.318		$6f_{5/2}$–$7d_{3/2}$	21.79	17.97
$8p_{1/2}$–$8d_{3/2}$	5.908	6.845	6.981	$7p_{1/2}$–$10s_{1/2}$	0.687	0.661		$6f_{5/2}$–$7d_{5/2}$	5.926	4.935
$8p_{3/2}$–$8d_{3/2}$	3.969	4.382	4.489	$7p_{1/2}$–$11s_{1/2}$	0.449	0.433		$6f_{7/2}$–$7d_{5/2}$	26.50	22.08
$8p_{3/2}$–$8d_{5/2}$	11.54	12.66	12.97	$7p_{1/2}$–$9d_{3/2}$	1.434	1.498		$6f_{5/2}$–$8d_{3/2}$	46.40	46.67
$8s_{1/2}$–$8p_{1/2}$	12.62	12.00	11.84	$7p_{1/2}$–$10d_{3/2}$	1.043	1.077		$6f_{5/2}$–$8d_{5/2}$	12.36	12.44
$8s_{1/2}$–$8p_{3/2}$	16.51	15.71	15.42	$7p_{3/2}$–$9d_{3/2}$	0.781	0.777		$6f_{7/2}$–$8d_{5/2}$	55.30	55.66
$8s_{1/2}$–$9p_{1/2}$	1.597	1.537	1.586	$7p_{3/2}$–$10d_{5/2}$	1.650	1.629		$9p_{1/2}$–$7d_{3/2}$	7.953	6.605
$9s_{1/2}$–$9p_{1/2}$	20.41	19.66		$9s_{1/2}$–$9p_{3/2}$	26.43	25.44		$9p_{3/2}$–$7d_{3/2}$	2.564	2.034
$10s_{1/2}$–$9p_{1/2}$	20.54	20.06		$10s_{1/2}$–$9p_{3/2}$	33.48	32.71		$10p_{1/2}$–$7d_{3/2}$	2.406	2.092
$10s_{1/2}$–$10p_{1/2}$	29.99	29.09		$10s_{1/2}$–$10p_{3/2}$	38.59	37.36		$10p_{1/2}$–$8d_{3/2}$	13.49	11.39
$10p_{3/2}$–$7d_{5/2}$	2.625	2.205		$10p_{3/2}$–$8d_{3/2}$	4.393	3.549		$10p_{3/2}$–$8d_{5/2}$	13.69	11.30

structure energy of $6p$ states differs from the experimental values 1.87%. The biggest difference between our CCSD results and experimental values for other energies is less than 0.5%.

B. Reduced matrix elements

There are 210 electric dipole transition matrix elements among the above mentioned states. Here we just list some of interesting reduced dipole matrix elements, which are relevant to the lifetimes and polarizabilities. Table II presents DF (denoted by Z_{DF}) and CCSD results (denoted by Z_{CCSD}) of the reduced dipole matrix elements, together with a comparison with the all-order results (denoted by Z_{LCCSD}) by Safronova *et al.* [32]. The differences between Z_{CCSD} and Z_{DF} are due to the electron correlation effects. The differences between Z_{CCSD} and Z_{LCCSD} is due to the contributions from the nonlinear terms of single- and double-cluster operators. From Table II, we observe that the differences between Z_{CCSD} and Z_{LCCSD} are about 1%–4% for most of the transitions. For those transitions that are sensitive to the electron correlations, the differences between Z_{CCSD} and Z_{LCCSD} are rather obvious. For example, the difference is about 10% for the $8p_{3/2}$–$6d$ transition. These differences imply that the inclusion of higher-order correlations involving nonlinear terms and triple excitations is important for achieving higher-accuracy results.

C. Lifetimes

Using the above calculated matrix elements, we determine the lifetimes for the ns ($n = 7$–10), np ($n = 7$–10), nd ($n = 6$–8), and nf ($n = 5$–6) states. The results are listed in Table III. The recommended values are obtained by using the CCSD matrix elements and experimental transition energies. Since the differences between Z_{CCSD} and Z_{LCCSD}

TABLE III. Radiative lifetimes of Tl in nanoseconds and comparison with other theoretical and experimental values. Uncertainties are given in parentheses.

Level	Theory (present)	Theory (others)	Expt.
$7s_{1/2}$	7.24(30)	7.43[a],7.17[b] 6.79[d]	7.45(20)[c],7.3(4)[d] 7.4(5)[e]
$7p_{1/2}$	60.1(2.5)	61.8[a],61.0[b] 60.21(55)[f]	63.1(1.7)[g]
$7p_{3/2}$	46.4(1.9)	47.3[a],47.4[b] 46.44(42)[f]	48.6(1.3)[g]
$6d_{3/2}$	6.09(25)	7.04[b],5.9[d]	8.5(5)[d],6.9(5)[e]
$6d_{5/2}$	7.24(29)	8.06[b],11.09[d]	7.2(6)[e]
$8s_{1/2}$	21.96(90)	20.9[b],21.59[d]	20(3)[e],25(2)[f]
$8p_{1/2}$	179.5(7.4)	177.6[a],185.0[b] 157.4[d]	184.1(4.0)[g]
$8p_{3/2}$	124.2(5.2)	123.5[a],130.0[b] 125.3 [43]	127.7(4.9)[g]
$7d_{3/2}$	15.21(62)	17.5[b],16.48[d]	20.5(1.5)[d],16.0(1.3)[e]
$7d_{5/2}$	18.31(75)	20.5[b],27.25[d]	19.8(1.5)[e]
$5f_{5/2}$	62.3(2.6)		
$5f_{7/2}$	62.8(2.6)		
$9s_{1/2}$	49.2(2.0)	46.0[b],57.03[d]	54(4),43(4)[e]
$9p_{1/2}$	368(15)	375.1[a],380.0[b] 323.1[d]	391.1(21.8)
$9p_{3/2}$	253(10)	251.3[a],267.0[b] 277.2[d]	273.6(13.5)
$8d_{3/2}$	30.6(1.3)	35.0[b],37.12[d]	45(5)[d],34(3)[e]
$8d_{5/2}$	36.9(1.5)	41.3[b],57.93[d]	44(4)[e]
$6f_{5/2}$	116(5)		
$6f_{7/2}$	118(5)		
$10s_{1/2}$	92(8)	86.1[b],53.32[d]	54(4)[d],31(3)[e]
$10p_{1/2}$	648(26)	570.6[d]	656.8(14.5)[g]
$10p_{3/2}$	449(18)	509.4[d]	480.8(31.6)[g]

[a][32]
[b][41]
[c][42]
[d][43]
[e][44]
[f][29]
[g][45]

for the transitions which strongly dominate lifetimes and polarizabilities are in 2%, we evaluate the uncertainties by setting ±2% variation of the CCSD matrix elements. We also compare our results with previously reported calculations and measurements in Table III [29,32,41–45]. From Table III, one can see that our lifetime of the $7s_{1/2}$ state is in agreement with the experimental values [42–44]. Our recommended lifetimes of the $7p_{1/2}$ and $7p_{3/2}$ states are shorter than the experimental values [45], but are in perfect agreement with the newest ones determined by combining the all-order calculations and experimental data [29]. For other p states, our results are in agreement with the experimental values of James *et al.* [45]. Safronova *et al.* employed the all-order method to evaluate the lifetimes of $7s$ and np ($n = 7$–9) [32], where our recommended values are close to theirs. For other s and d states, it is seen that there are obvious differences among our results and two other theoretical results obtained by semiempirical models [41,43] and the experimental values [43,44]. To the best of our knowledge, there are no available *ab initio* calculations for d- and f-state lifetimes.

D. Static polarizabilities

Table IV lists the contributions of individual transitions to the static scalar dipole polarizabilities of the $6p$, $7s$, $7p$, $8s$, $8p$, and $6d$ states. The recommended values and uncertainties of the polarizabilities are given in the same way as for the lifetimes. The contributions from transitions not explicitly listed in the table and from the core-valence correlation $\alpha_{cv}^{(1)}$ are labeled "Others," which are obtained by DFCP calculation. From Table IV, one can see that the dominating contributions to the $7s_{1/2}$-, $7p_{1/2}$-, $8p_{1/2}$-, and $8p_{3/2}$-state scalar polarizabilities, which are larger than 85%, are from one or two specific transitions. The $7s$–$7p_{1/2}$ and $7s$–$7p_{3/2}$ transitions contribute 102% of the total $7s$-state polarizability. The $7s$-$7p_{1/2}$ and $7s$-$7p_{3/2}$ transition matrix elements may be derived by combining a measured $7s$-state static dipole polarizability with theoretical results of other contributions and the ratio between the line strengths of the $7s$–$7p_{1/2}$ and $7s$–$7p_{3/2}$ transitions, which has been demonstrated by Safronova and Majumder [29]. There is only one transition that dominates the scalar dipole polarizabilities of the $7p_{1/2}$, $8p_{1/2}$, and $8p_{3/2}$ states. For the $7p_{1/2}$-state scalar dipole polarizability, the $7p_{1/2}$-$6d_{3/2}$ transition contributes 87% of the total. For the $8p_{1/2}$ state, the $8p_{1/2}$–$7d_{3/2}$ transition contributes 94% of the total. For the $8p_{3/2}$ state, the $8p_{3/2}$–$7d_{5/2}$ transition contributes 92% of the total. The scalar dipole polarizabilities of these three states are larger than the $6p_{1/2}$ state by at least two orders of magnitude. The $7p_{1/2}$–$6d_{3/2}$, $8p_{1/2}$–$7d_{3/2}$, and $8p_{3/2}$–$7d_{5/2}$ transition matrix elements can be derived by measuring the scalar dipole polarizabilities of $7p_{1/2}$, $8p_{1/2}$, and $8p_{3/2}$ states, respectively. The experiment techniques, which have been applied to the measurements of the polarizabilities of $6p_{1/2}$ [30], $7p_{1/2}$, and $7p_{3/2}$ states of the In atom [31] can be extended to the Tl atom.

Table V lists the contributions of individual transitions to the static tensor dipole polarizabilities of $6p_{3/2}$, $7p_{3/2}$, $8p_{3/2}$, $6d_{3/2}$, and $6d_{5/2}$ states. From Table V, one can see that there are cancellations among the dominant transitions. The tensor polarizabilities of $6d$ states are positive, but the ones of other states are negative, which is opposite for the case of scalar polarizabilities.

Table VI is a comparison of the present polarizabilities with available theoretical and experimental values. For the ground state, our value for $\alpha_0^{(1)}$ is 49.2(2.0), which is in agreement with the value 49.2 by Kozlov *et al.* [21], with the value 48.81 by Dzuba and Flambaum [22] using the RCI+MBPT method, with the value 52.1(1.6) of Borschevsky *et al.* using the finite field coupled-cluster method [28], with the value 50.0(1.0) of Safronova and Majumder using an all-order method [29], and with the experimental value 51(7) [29]. For the $6p_{3/2}$ state, our result of $\alpha_0^{(1)}$ agrees with the result by Kozlov *et al.* [21], but our recommended value $\alpha_t^{(1)} = -26.7$ is smaller than their result −25.0. We also give the polarizabilities of the $6p_{3/2}$ state for different magnetic projection m_j, in order to compare with the results obtained by the finite field coupled-cluster method [28]. An agreement is observed between our results and the finite field results.

TABLE IV. Contributions of individual transitions to the static scalar dipole polarizabilities of $6p$, $7s$, $7p$, $8s$, $8p$, and $6d$ states. Uncertainties are given in parentheses.

Contr.	$\alpha_0^{(1)}$	Contr.	$\alpha_0^{(1)}$	Contr.	$\alpha_0^{(1)}$	Contr.	$\alpha_0^{(1)}$	Contr.	$\alpha_0^{(1)}$
	$6p_{1/2}$		$7s_{1/2}$		$7p_{1/2}$		$8s_{1/2}$		$8p_{1/2}$
$7s_{1/2}$	9.07(37)	$6p_{1/2}$	−9	$7s_{1/2}$	−345(14)	$7p_{1/2}$	−616(26)	$8s_{1/2}$	−4021(162)
$8s_{1/2}$	0.55(2)	$7p_{1/2}$	345(14)	$8s_{1/2}$	616(26)	$8p_{1/2}$	4021(162)	$9s_{1/2}$	6101(246)
$9s_{1/2}$	0.15(1)	$8p_{1/2}$	2	$9s_{1/2}$	13(1)	$9p_{1/2}$	31(1)	$10s_{1/2}$	93(4)
$6d_{3/2}$	11.89(48)	$6p_{3/2}$	−45(2)	$6d_{3/2}$	4331(174)	$7p_{3/2}$	−2262(91)	$6d_{3/2}$	−126(5)
$7d_{3/2}$	2.36(10)	$7p_{3/2}$	548(22)	$7d_{3/2}$	205(8)	$8p_{3/2}$	6029(243)	$7d_{3/2}$	58 628(2369)
$8d_{3/2}$	0.87(3)	$8p_{3/2}$	10(1)	$8d_{3/2}$	38(2)	$9p_{3/2}$	110(4)	$8d_{3/2}$	1037(42)
$9d_{3/2}$	0.42(2)	$9p_{3/2}$	2	$9d_{3/2}$	14	$10p_{3/2}$	20(1)	$9d_{3/2}$	179(6)
Others	4.3(1.0)	Others	5(1)	Others	55(4)	Others	34(1)	Others	264(5)
Core	19.60	Core	19.60	Core	19.60	Core	19.60	Core	19.60
Total	49.2(2.0)	Total	878(34)	Total	4946(201)	Total	7387(297)	Total	62 174(2503)
	$6p_{3/2}$		$7p_{3/2}$		$6d_{3/2}$		$6d_{5/2}$		$8p_{3/2}$
$7s_{1/2}$	22.61(91)	$7s_{1/2}$	−274(11)	$6p_{1/2}$	−6(1)	$6p_{3/2}$	-15(1)	$8s_{1/2}$	−3015(121)
$8s_{1/2}$	0.76(3)	$8s_{1/2}$	1131(46)	$7p_{1/2}$	−2165(88)	$7p_{3/2}$	−5062(204)	$9s_{1/2}$	10 499(423)
$9s_{1/2}$	0.19(1)	$9s_{1/2}$	12(1)	$8p_{1/2}$	63(2)	$8p_{3/2}$	37(1)	$10s_{1/2}$	73(3)
$6d_{3/2}$	2.65(10)	$6d_{3/2}$	897(36)	$9p_{1/2}$	4	$9p_{3/2}$	3	$7d_{3/2}$	14 122(571)
$7d_{3/2}$	0.42(2)	$7d_{3/2}$	44(2)	$7p_{3/2}$	−897(36)	$5f_{5/2}$	55(2)	$8d_{3/2}$	239(10)
$6d_{5/2}$	22.96(93)	$6d_{5/2}$	7593(307)	$8p_{3/2}$	5(1)	$6f_{5/2}$	5	$6d_{5/2}$	−55(2)
$7d_{5/2}$	3.69(14)	$7d_{5/2}$	371(15)	$5f_{5/2}$	1098(45)	$5f_{7/2}$	1094(44)	$7d_{5/2}$	113 205(4573)
$8d_{5/2}$	1.25(5)	$8d_{5/2}$	54(2)	$6f_{5/2}$	105(4)	$6f_{7/2}$	101(4)	$8d_{5/2}$	1987(81)
$9d_{5/2}$	0.58(2)	$9d_{5/2}$	18(1)	$7f_{5/2}$	29(1)	$7f_{7/2}$	28(1)	$9d_{5/2}$	266(10)
$10d_{5/2}$	0.32(1)	$10d_{5/2}$	8	$8f_{5/2}$	12	$8f_{7/2}$	11	$10d_{5/2}$	84(3)
Others	5.0(1.0)	Others	60(2)	Others	47(2)	Others	44(2)	Others	237(2)
Core	19.60	Core	19.60	Core	19.60	Core	19.60	Core	19.60
Total	80.0(3.2)	Total	9934(398)	Total	−1685(70)	Total	−3679(151)	Total	137 690(5553)

Our results for the $7s_{1/2}$, $7p_{1/2}$ states and for the $6p_{1/2}$-$7s_{1/2}$ and $6p_{1/2}$-$7p_{1/2}$ transitions are consistent with the theoretical results of Ref. [29] and experimental results of Refs. [25,26]. There are no available data for $7p_{3/2}$-, $8s$-, $8p$-, and $6d$-state polarizabilities.

Table VII gives the Stark-induced scalar $\alpha_s^{(1)}$ and vector $\beta_s^{(1)}$ dipole polarizabilities for the $6p_{1/2}$-$7p_{1/2}$ transition, and a comparison with available results [24,25,27]. The detailed expressions of $\alpha_s^{(1)}$ and $\beta_s^{(1)}$ can be found in Ref. [27]. We can see from this table that the differences between our recommended values and the all-order results of Safronova *et al.* [27] are about 5.4% for $\alpha_s^{(1)}$ and 2.7% for $\beta_s^{(1)}$. As shown in Table VII, the main difference is from the $6d_{3/2}$ state. The reason for this discrepancy is that our result 2.423 for the $6p_{1/2}$–$6d_{3/2}$ transition matrix element is larger than the value 2.334 of Safronova *et al.* by about 4%. Also the two experimental results are in disagreement. The two theoretical results are closer to the value measured by Demille *et al.* [25] than the one by Tanner *et al.* [24]. Our polarizabilities are consistent with the experimental values by Demille *et al.*, but the ratio $\beta_s^{(1)}/\alpha_s^{(1)} = 0.79$ is smaller than the measured value 0.83(1) of Demille *et al.* [25].

TABLE V. Contributions of individual transitions to the static tensor dipole polarizabilities of $6p_{3/2}$, $7p_{3/2}$, $8p_{3/2}$, $6d_{3/2}$, and $6d_{5/2}$ states. Uncertainties are given in parentheses.

Contr.	$\alpha_t^{(1)}$	Contr.	$\alpha_t^{(1)}$	Contr.	$\alpha_t^{(1)}$	Contr.	$\alpha_t^{(1)}$	Contr.	$\alpha_t^{(1)}$
	$6p_{3/2}$		$7p_{3/2}$		$6d_{3/2}$		$6d_{5/2}$		$8p_{3/2}$
$7s_{1/2}$	−22.61(91)	$7s_{1/2}$	274(11)	$6p_{1/2}$	6(1)	$6p_{3/2}$	15(1)	$8s_{1/2}$	3015(121)
$8s_{1/2}$	−0.76(3)	$8s_{1/2}$	−1131(46)	$7p_{1/2}$	2165(88)	$7p_{3/2}$	5062(204)	$9s_{1/2}$	−10 499(423)
$9s_{1/2}$	−0.19(1)	$9s_{1/2}$	−12(1)	$8p_{1/2}$	−63(3)	$8p_{3/2}$	−37(1)	$10s_{1/2}$	−73(3)
$6d_{3/2}$	2.12(8)	$6d_{3/2}$	717(29)	$7p_{3/2}$	−717(29)	$5f_{5/2}$	63(2)	$7d_{3/2}$	11 298(456)
$7d_{3/2}$	0.33(1)	$7d_{3/2}$	35(2)	$8p_{3/2}$	4	$6f_{5/2}$	6	$8d_{3/2}$	192(7)
$6d_{5/2}$	−4.59(18)	$6d_{5/2}$	−1518(61)	$5f_{5/2}$	−220(9)	$5f_{7/2}$	−391(16)	$7d_{5/2}$	−22 641(915)
$7d_{5/2}$	−0.74(3)	$7d_{5/2}$	−74(3)	$6f_{5/2}$	−21(1)	$6f_{7/2}$	−36(2)	$8d_{5/2}$	−397(17)
$8d_{5/2}$	−0.25(1)	$8d_{5/2}$	−11(1)	$7f_{5/2}$	−6	$7f_{7/2}$	−10	$9d_{5/2}$	−53(2)
Others	−0.1(1.0)	Others	−8(1)	Others	18(1)	Others	17(2)	Others	−19(2)
Total	−26.7(2.0)	Total	−1728(71)	Total	1130(47)	Total	4655(188)	Total	−19 177(773)

TABLE VI. Comparison of the present polarizabilities with available theoretical and experimental values. Uncertainties are given in parentheses.

States		Theory (present)	Theory (others)	Expt.
$6p_{1/2}$	$\alpha_0^{(1)}$	49.2(2.0)	49.2[a],48.81[b]	51(7)[d]
			52.1(1.6)[c]	
			50.0(1.0)[d]	
$6p_{3/2}$	$\alpha_0^{(1)}$	80.0(3.2)	79.6[a]	
	$\alpha_t^{(1)}$	−26.7(2.0)	−25.0[a]	
	$\alpha_{1/2}^{(1)}$	106.7(3.3)	105.0(5.3)[c]	
	$\alpha_{3/2}^{(1)}$	53.3(1.2)	55.7(2.8)[c]	
$7s_{1/2}$	$\alpha_0^{(1)}$	878(34)	881(9)[d]	
$7p_{1/2}$	$\alpha_0^{(1)}$	4946(201)	4918(120)[d]	
$6p_{1/2}$–$7s_{1/2}$	$\Delta\alpha$	−829(33)	−831(8)[d]	−900(48)[e]
				−829.7(3.1)[f]
$6p_{1/2}$–$7p_{1/2}$	$\Delta\alpha$	−4897(196)	−4868(120)[d]	−4968(249)[e]

[a][21]
[b][22]
[c][28]
[d][29]
[e][25]
[f][26]

E. Magic wavelengths

The magic wavelength for a transition is the wavelength for which the ac Stark shift to the transition energy is zero. The magic wavelengths are found at the crossings of the two dynamic polarizability curves associated with the two states in the transition. The dynamic polarizabilities for the $7s_{1/2}$ and $6p_{1/2}$ states of Tl are shown in Fig 1. There are eight magic wavelengths found in the range of 488–1302 nm, which are indicated by the arrows. The longest magic wavelength 1245.15 nm lies in the $7s_{1/2}$–$7p_{1/2}$ and $7s_{1/2}$–$7p_{3/2}$ transitions. Other magic wavelengths occur near the resonant position of $7s-np$ ($n=8$–11). In the same range, the dynamic polarizabilities for the $7s_{1/2}$ and $6p_{3/2}$ states of Tl are shown in Fig. 2, and the magic wavelengths are also indicated by the arrows. These figures assume linear polarized light. From Fig. 2, we observe that the first seven magic wavelengths for two magnetic sublevels occur at the same resonant position. For the $7s_{1/2}$–$6p_{3/2,|m_j|=3/2}$ transition, there are two additional magic wavelengths near 496 nm and 492 nm lying between the $7s_{1/2}$–$10_{3/2}$ and $7s_{1/2}$–$11p_{1/2}$ transitions. All magic wavelengths and the corresponding polarizabilities at the magic wavelengths are listed in Table VIII.

Among these magic wavelengths, the magic wavelength near 1245 nm is special. Table IX gives the contributions of individual transitions to the dynamic polarizabilities of $7s_{1/2}$, $6p_{1/2}$, and $6p_{3/2}$ states near 1245 nm. From Table IX, one can find that there is a rather strong cancellation between the $7p_{1/2}$- and $7p_{3/2}$-state contributions to the $7s$ dynamic polarizability at these wavelengths. The situation here is similar to the magic wavelength near 395 nm for the Ca^+ clock transition [14]. Experimental measurements on these

TABLE VII. Stark-induced scalar $\alpha_s^{(1)}$ and vector $\beta_s^{(1)}$ dipole polarizabilities for the $6p_{1/2}$–$7p_{1/2}$ transition. Uncertainties are given in parentheses.

	$\alpha_s^{(1)}$		$\beta_s^{(1)}$	
Contr.	Present	Ref. [27]	Present	Ref. [27]
$7s_{1/2}$	−36.9(1.4)	−37.2	−67.0(2.7)	−67.5
$8s_{1/2}$	−29.9(1.3)	−29.7	−23.6(1.0)	−23.4
$9s_{1/2}$	−1.9(1)	−1.9	−1.3(1)	−1.2
$10s_{1/2}$	−0.5(1)	−0.5	−0.3(1)	−0.3
$11s_{1/2}$	−0.2(1)		−0.1(1)	
$6d_{3/2}$	514(21)	492.0	−231(9)	−220.7
$7d_{3/2}$	−30.2(1.3)	−29.4	10.4(4)	10.1
$8d_{3/2}$	−7.3(3)	−6.9	2.3(1)	2.1
$9d_{3/2}$	−3.0(1)	−2.8	0.9(1)	0.8
$10d_{3/2}$	−1.5(1)		0.4(1)	
Others	−13.9(2)	−15.7	3.4(2)	2.4
Total	388(16)	368	−306(13)	−298
Expt. [24]	247(12)		−198(10)	
Expt. [25]	377(8)		−313(8)	

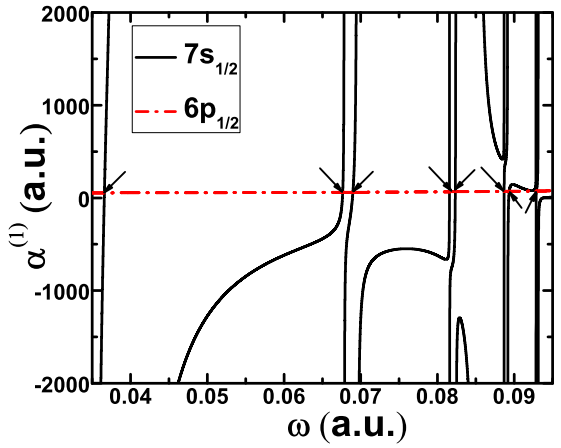

FIG. 1. Dynamic polarizabilities of the $7s_{1/2}$ and $6p_{1/2}$ states of Tl. The magic wavelengths are indicated by the arrows.

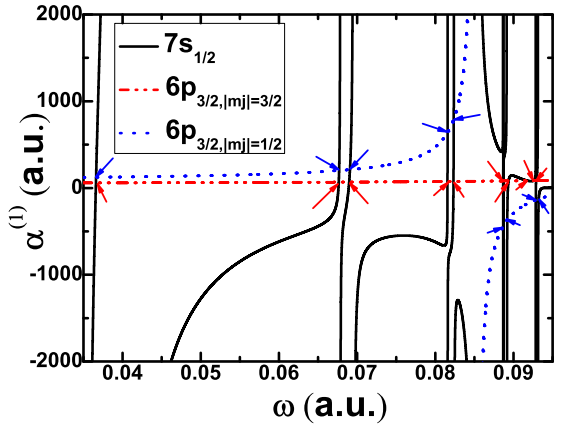

FIG. 2. Dynamic polarizabilities of the $7s_{1/2}$ and $6p_{3/2}$ states of Tl. The magic wavelengths are indicated by the arrows.

TABLE VIII. Magic wavelengths in nanometers for the $7s_{1/2} - 6p_{1/2}$ and $7s_{1/2} - 6p_{3/2}$ transitions.

Resonance		$7s_{1/2}$–$6p_{1/2,\|m_j\|=1/2}$		$7s_{1/2}$–$6p_{3/2,\|m_j\|=3/2}$		$7s_{1/2}$–$6p_{3/2,\|m_j\|=1/2}$	
Transition	λ_{res}	λ_{magic}	$\alpha(\lambda_{magic})$	λ_{magic}	$\alpha(\lambda_{magic})$	λ_{magic}	$\alpha(\lambda_{magic})$
$7s_{1/2}$–$7p_{1/2}$	1301.676						
		1245.149(1)	50.0(1.1)	1245.104(1)	54.8(1.2)	1244.495(1)	119(4)
$7s_{1/2}$–$7p_{3/2}$	1151.596						
		673.686(1)	55.5(1.3)	673.650(1)	62.5(1.5)	673.127(1)	201(7)
$7s_{1/2}$–$8p_{1/2}$	671.564						
		660.659(1)	56.0(1.3)	660.600(1)	63.1(1.5)	659.626(1)	211(8)
$7s_{1/2}$–$8p_{3/2}$	655.166						
		558.676(1)	61.1(1.5)	558.674(1)	70.2(1.9)	558.623(1)	639(15)
$7s_{1/2}$–$9p_{1/2}$	558.553						
		553.489(1)	61.5(1.5)	553.484(1)	70.8(2.0)	553.262(1)	793(31)
$7s_{1/2}$–$9p_{3/2}$	552.944						
$7s_{1/2}$–$10p_{1/2}$	513.827						
		513.740(1)	65.5(1.7)	513.737(1)	76.2(2.1)	513.793(1)	−436.13
$7s_{1/2}$–$10p_{3/2}$	511.088						
		509.882(2)	66.0(1.8)	509.784(3)	76.9(2.1)	510.775(1)	−366(16)
				496.45(7)	79.5(2.2)		
				492.38(8)	80.4(2.2)		
$7s_{1/2}$–$11p_{1/2}$	490.766						
		490.474(3)	69.1(1.8)	490.406(7)	80.9(2.2)	490.717(1)	−137(8)
$7s_{1/2}$–$11p_{3/2}$	489.246					488.670(4)	−124(7)

magic wavelengths near 1245 nm would give estimates for the $7s_{1/2}$–$7p_{1/2}$ and $7s_{1/2}$–$7p_{3/2}$ line strengths and their ratio.

A parameter related to the magic wavelength is the tune-out wavelength. The tune-out wavelengths for an atomic state are the wavelengths at which the polarizability for that state goes to zero. We determined the longest tune-out wavelength of the $6p_{1/2}$ state of Tl. This tune-out wavelength is 354.85 nm, which lies in the $6p_{1/2}$–$7s_{1/2}$ and $6p_{1/2}$–$5d_{3/2}$ transitions. We hope that this tune-out wavelength and above magic wavelengths will be useful for further PNC, EDM, and high-precision measurements based on the Tl atom.

TABLE IX. Contributions of individual transitions to the dynamic polarizabilities of $7s_{1/2}$, $6p_{1/2}$, and $6p_{3/2}$ states near 1245 nm.

λ_{magic}	1245.149		1245.104		1244.495
	$7s_{1/2}$		$7s_{1/2}$	$7s_{1/2}$	
$6p_{1/2}$	−9.99	$6p_{1/2}$	−9.99	$6p_{1/2}$	−9.99
$7p_{1/2}$	**–3714.96**	$7p_{1/2}$	**–3711.81**	$7p_{1/2}$	**–3669.60**
$8p_{1/2}$	3.35	$8p_{1/2}$	3.35	$8p_{1/2}$	3.35
$6p_{3/2}$	−55.48	$6p_{3/2}$	−55.48	$6p_{3/2}$	−55.49
$7p_{3/2}$	**3785.79**	$7p_{3/2}$	**3787.40**	$7p_{3/2}$	**3809.45**
$8p_{3/2}$	14.33	$8p_{3/2}$	14.33	$8p_{3/2}$	14.33
Others	7.36	Others	7.36	Others	7.36
Core	19.60	Core	19.60	Core	19.60
Total	50.00	Total	54.76	Total	119.01
	$6p_{1/2}$		$6p_{3/2,\|m_j\|=3/2}$		$6p_{3/2,\|m_j\|=1/2}$
$7s_{1/2}$	9.99	$6d_{3/2}$	5.18	$7s_{1/2}$	55.49
$6d_{3/2}$	12.51	$6d_{5/2}$	19.96	$6d_{5/2}$	29.95
$7d_{3/2}$	2.45	$7d_{5/2}$	3.12	$7d_{5/2}$	4.68
Others	5.45	Others	6.70	Others	9.29
Core	19.60	Core	19.60	Core	19.60
Total	50.00	Total	54.76	Total	119.01

V. SUMMARY

We have employed the relativistic coupled-cluster method to calculate energies, transition matrix elements, lifetimes, and polarizability-related properties of Tl. The trivalent Tl atom has been computationally treated as a monovalent system, together with all linear and nonlinear terms of single- and double-cluster operators included in the correlation calculations. For static dipole polarizabilities, we have observed that the dominating contributions of the static scalar polarizabilities for $7s_{1/2}$, $7p_{1/2}$, $8p_{1/2}$, and $8p_{3/2}$ states are from one or two specific transitions. The $7p_{1/2}$–$6d_{3/2}$, $8p_{1/2}$–$7d_{3/2}$, and $8p_{3/2}$–$7d_{5/2}$ transition matrix elements can be derived by combining experimentally measured scalar dipole polarizabilities of the $7p_{1/2}$, $8p_{1/2}$, and $8p_{3/2}$ states. The two-step diode laser spectroscopy method, which has been used for the measurement of the polarizabilities of $6p_{1/2}$, $7p_{1/2}$, and $7p_{3/2}$ states of the In atom, may be applied to the Tl atom. The static polarizabilities of $7p_{3/2}$, $8s$, $8p$, and $6d$ states have been reported in this paper for the first time. The magic wavelengths of $6p_{1/2}$–$7s$ and $6p_{3/2}$–$7s$ transitions and the longest tune-out wavelength of the $6p_{1/2}$ state have also been identified by evaluating the dynamic polarizabilities of $6p$ and $7s$ states. These magic wavelengths and tune-out wavelength may be useful for further Tl experiments. Among these magic wavelengths, the magic wavelength near 1245 nm is a special one. Experimental measurements on the magic wavelengths near 1245 nm for the $7s$–$6p_{1/2}$ and $7s$–$6p_{3/2}$ transitions could give estimates for the $7s_{1/2}$–$7p_{1/2}$ and $7s_{1/2}$–$7p_{3/2}$ line strengths and their ratio.

ACKNOWLEDGMENTS

We are grateful to Prof. Z.-C. Yan for many useful suggestions and reading our manuscript. We would also like to thank anonymous referees for their valuable suggestions. This work was supported by National Natural Science Foundation of China Grants No. 11504094 and No. 91536102, Chinese Academy of Sciences Grant No. XDB21030300, and China Postdoctoral Science Foundation Grant No. 2017M622556.

[1] J. Mitroy, M. S. Safronova, and C. W. Clark, J. Phys. B: At. Mol. Phys. **43**, 202001 (2010).

[2] K. Beloy, N. Hinkley, N. B. Phillips, J. A. Sherman, M. Schioppo, J. Lehman, A. Feldman, L. M. Hanssen, C. W. Oates, and A. D. Ludlow, Phys. Rev. Lett. **113**, 260801 (2014).

[3] P. Dubé, A. A. Madej, M. Tibbo, and J. E. Bernard, Phys. Rev. Lett. **112**, 173002 (2014).

[4] A. Derevianko and H. Katori, Rev. Mod. Phys. **83**, 331 (2011).

[5] A. D. Ludlow, M. M. Boyd, J. Ye, E. Peik, and P. O. Schmidt, Rev. Mod. Phys. **87**, 637 (2015).

[6] P. M. Duarte, R. A. Hart, J. M. Hitchcock, T. A. Corcovilos, T.-L. Yang, A. Reed, and R. G. Hulet, Phys. Rev. A **84**, 061406 (2011).

[7] D. C. McKay, D. Jervis, D. J. Fine, J. W. Simpson-Porco, G. J. A. Edge, and J. H. Thywissen, Phys. Rev. A **84**, 063420 (2011).

[8] M. S. Safronova, U. I. Safronova, and C. W. Clark, Phys. Rev. A **86**, 042505 (2012).

[9] M. S. Safronova, U. I. Safronova, and C. W. Clark, Phys. Rev. A **87**, 052504 (2013).

[10] L. J. LeBlanc and J. H. Thywissen, Phys. Rev. A **75**, 053612 (2007).

[11] B. Arora, M. S. Safronova, and C. W. Clark, Phys. Rev. A **84**, 043401 (2011).

[12] W. F. Holmgren, R. Trubko, I. Hromada, and A. D. Cronin, Phys. Rev. Lett. **109**, 243004 (2012).

[13] C. D. Herold, V. D. Vaidya, X. Li, S. L. Rolston, J. V. Porto, and M. S. Safronova, Phys. Rev. Lett. **109**, 243003 (2012).

[14] Y.-B. Tang, H.-X. Qiao, T.-Y. Shi, and J. Mitroy, Phys. Rev. A **87**, 042517 (2013).

[15] P.-L. Liu, Y. Huang, W. Bian, H. Shao, H. Guan, Y.-B. Tang, C.-B. Li, J. Mitroy, and K.-L. Gao, Phys. Rev. Lett. **114**, 223001 (2015).

[16] J. Mitroy and L.-Y. Tang, Phys. Rev. A **88**, 052515 (2013).

[17] B. M. Henson, R. I. Khakimov, R. G. Dall, K. G. H. Baldwin, L.-Y. Tang, and A. G. Truscott, Phys. Rev. Lett. **115**, 043004 (2015).

[18] Y.-H. Zhang, L.-Y. Tang, X.-Z. Zhang, and T.-Y. Shi, Phys. Rev. A **93**, 052516 (2016).

[19] P. A. Vetter, D. M. Meekhof, P. K. Majumder, S. K. Lamoreaux, and E. N. Fortson, Phys. Rev. Lett. **74**, 2658 (1995).

[20] B. C. Regan, E. D. Commins, C. J. Schmidt, and D. DeMille, Phys. Rev. Lett. **88**, 071805 (2002).

[21] M. G. Kozlov, S. G. Porsev, and W. R. Johnson, Phys. Rev. A **64**, 052107 (2001).

[22] V. A. Dzuba and V. V. Flambaum, Phys. Rev. A **80**, 062509 (2009).

[23] S. G. Porsev, M. S. Safronova, and M. G. Kozlov, Phys. Rev. Lett. **108**, 173001 (2012).

[24] C. E. Tanner and E. D. Commins, Phys. Rev. Lett. **56**, 332 (1986).

[25] D. De Mille, D. Budker, and E. D. Commins, Phys. Rev. A **50**, 4657 (1994).

[26] S. C. Doret, P. D. Friedberg, A. J. Speck, D. S. Richardson, and P. K. Majumder, Phys. Rev. A **66**, 052504 (2002).

[27] M. S. Safronova, W. R. Johnson, U. I. Safronova, and T. E. Cowan, Phys. Rev. A **74**, 022504 (2006).

[28] A. Borschevsky, T. Zelovich, E. Eliav, and U. Kaldor, Chem. Phys. **395**, 104 (2012).

[29] M. S. Safronova and P. K. Majumder, Phys. Rev. A **87**, 042502 (2013).

[30] B. L. Augenbraun, A. Carter, P. M. Rupasinghe, and P. K. Majumder, Phys. Rev. A **94**, 022515 (2016).

[31] N. B. Vilas, B.-Y. Wang, P. M. Rupasinghe, D. L. Maser, M. S. Safronova, U. I. Safronova, and P. K. Majumder, Phys. Rev. A **97**, 022507 (2018).

[32] U. I. Safronova, M. S. Safronova, and W. R. Johnson, Phys. Rev. A **71**, 052506 (2005).

[33] H. Gharibnejad and A. Derevianko, Phys. Rev. A **86**, 022505 (2012).

[34] Z. Zuhrianda, M. S. Safronova, and M. G. Kozlov, Phys. Rev. A **85**, 022513 (2012).

[35] Y.-B. Tang, C.-B. Li, and H.-X. Qiao, Chin. Phys. B **23**, 063101 (2014).

[36] P. Pulay, Chem. Phys. Lett. **73**, 393 (1980).

[37] P. Pulay, J. Comput. Chem. **3**, 556 (1982).

[38] Y.-B. Tang, B.-Q. Lou, and T.-Y. Shi, Phys. Rev. A **96**, 022513 (2017).

[39] Y. Tang, Z. Zhong, C. Li, H. Qiao, and T. Shi, Phys. Rev. A **87**, 022510 (2013).

[40] A. Kramida, Y. Ralchenko, J. Reader, and NIST ASD Team, *NIST Atomic Spectra Database (Version 5.0.0)* (NIST, Gaithersburg, 2012).

[41] J. N. Bardsley and D. W. Norcross, J. Quant. Spectrosc. Radiat. Transfer **23**, 575 (1980).

[42] M. Norton and A. Gallagher, Phys. Rev. A **3**, 915 (1971).

[43] É. Biémont, P. Palmeri, P. Quinet, Z. Dai, S. Svanberg, and H. L. Xu, J. Phys. B At. Mol. Phys. **38**, 3547 (2005).

[44] L. L. Shimon and N. M. Erdevdi, Opt. Spectrosc. **42**, 137 (1977).

[45] J. V. James, C. C. Wang, and C. Doty, Phys. Rev. A **34**, 1117 (1986).